Coastal Lows along the Subtropical West Coast of South America: Mean Structure and Evolution

RENÉ D. GARREAUD, JOSÉ A. RUTLLANT, AND HUMBERTO FUENZALIDA

Department of Geophysics, Universidad de Chile, Santiago, Chile

(Manuscript received 22 November 2000, in final form 7 June 2001)

ABSTRACT

The typical conditions of the eastern boundary of the subtropical anticyclone [e.g., well-defined marine boundary layer (MBL), equatorward low-level flow] that prevail along the mountainous west coast of subtropical South America are frequently disrupted by shallow, warm-core low pressure cells with alongshore and cross-shore scales of 1000 and 500 km, respectively. These so-called coastal lows (CLs) occur up to five times per month in all seasons, although they are better defined from fall to spring. Marked weather changes along the coast and farther inland are associated with the transition from pressure drop to pressure rise.

The mean structure and evolution of CLs is documented in this work, using a compositing analysis of 57 episodes selected from hourly pressure observations at a coastal station at 30°S during the austral winters of 1991, 1993, and 1994, and concurrent measurements from a regional research network of nine automatic weather stations, NCEP–NCAR reanalysis fields and high-resolution visible satellite imagery. Coastal lows tend to develop as a migratory surface anticyclone approaches southern Chile at about 40°S producing a poleward-oriented pressure gradient and geostrophically balanced offshore component in the low-level wind. At subtropical latitudes the transition from negative to positive geopotential anomalies occurs around 850 hPa. Enhanced mid- and low-level subsidence near the coast and downslope flow over the coastal range and Andes Mountains leads to the replacement of the cool, marine air by adiabatically warmed air, lowering the surface pressure at the coast and offshore. As the midlatitude ridge moves to the east of the Andes, the alongshore pressure gradient reverts back and the easterly wind ceases to act. The recovery of the surface pressure toward mean values occurs as the cool, cloud-topped MBL returns to the subtropical coast, although the pressure rise can be attenuated by midlatitude troughing. The return of the MBL resembles a Kelvin wave propagating along the coast from northern Chile (where the MBL eventually thickened) into subtropical latitudes in about a day.

1. Introduction

The subtropical west coast of South America (north-central Chile; Fig. 1) is year-round under the influence of the southeast Pacific anticyclone that results in a semiarid climate, with a very stable lower troposphere, relatively cold sea surface temperature, and predominantly south-southwesterly wind along the coast. The well-defined marine atmospheric boundary layer (MBL), often topped by an extensive deck of coastal stratocumulus, is capped by a strong and persistent subsidence temperature inversion. At 30°S the coastal MBL is about 800 m deep, and the inversion layer has a thickness of about 600 m and a temperature increment of about 6°C (Rutllant 1994). This region is also characterized by its prominent topography: a coastal range that in many places rises above 1000-m elevation, and the Andes Cordillera that rises sharply to its top above 4000 m within 300 km of the coastline (Fig. 2). Under a wide range of static stabilities, low- and midlevel westerly flow is effectively blocked by these mountain ranges (Rutllant 1994).

Shallow, subsynoptic low pressure centers, not associated with the polar front, are frequently observed in this region and referred to as coastal lows (CLs; Rutllant 1983). At coastal stations the lows are identified by a transient (~2 days) drop of surface pressure (~10 hPa) at the same time that pressure is rising in the middle troposphere. The coastal pressure minimum generally exhibits a southward displacement in the 27°–37°S latitude span, reaching occasionally as far as 42°S in the austral summer (Rutllant and Garreaud 1995). The importance of CLs in terms of their related weather changes, from shallow MBL and sunny conditions at their leading edge (i.e., to the south of the pressure minimum) to overcast, cool, and moist conditions in connection with their trailing (northern) edge, has been the subject of a number of applied studies [e.g., on air pollution episodes in Santiago (Rutllant 1981; Rutllant and Garreaud 1995); on the occurrence of water-collection episodes from coastal stratocumulus (Fuenzalida et al. 1990); and on ocean upwelling–favorable wind events

Corresponding author address: Dr. René D. Garreaud, Department of Geophysics, Universidad de Chile, Blanco Encalada 2085, Santiago, Chile.
E-mail: rgarreau@dgf.uchile.cl

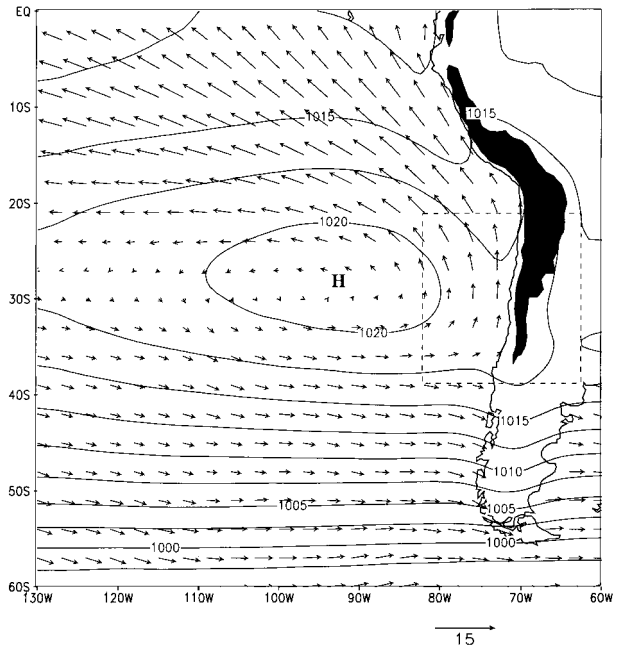

FIG. 1. Long-term mean SLP (contoured every 2.5 hPa) and surface winds (reference vector at the bottom, in m s^{-1}) for the austral winter (May–Sep). Data from NCEP–NCAR reanalysis (1979–98). Black area indicates terrain elevation in excess of 2000 m. Dashed box indicates area enlarged in Fig. 2.

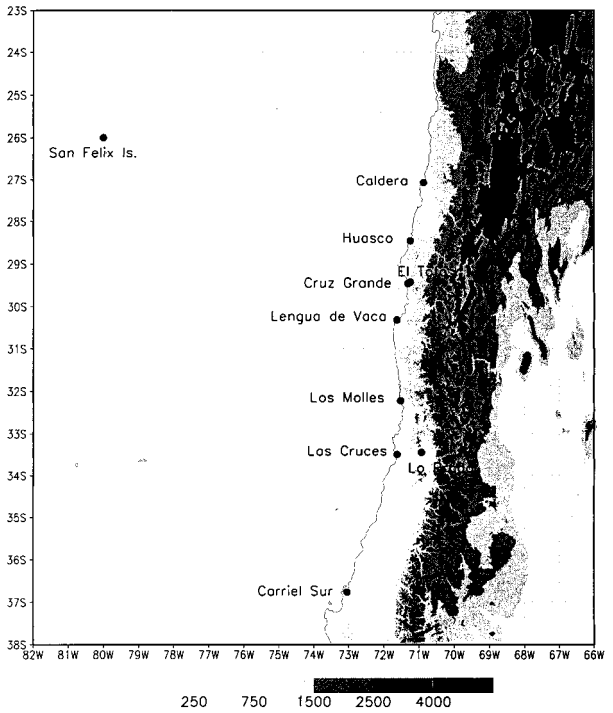

FIG. 2. Topographic map of north-central Chile (shading scale in m MSL). Key meteorological stations are indicated by a solid circle.

along the north-central coast of Chile (Rutllant 1993, 1997)].

Coastal lows or troughs have also been documented around the southern Africa coast (e.g., Gill 1982; Reason and Jury 1990). Furthermore, the recovery of the MBL along the coast at the demise stage of a CL (surface pressure rising) seems to share some of the typical features of coastally trapped disturbances (CTDs) along the mountainous western coast of North America (e.g., Dorman 1985; Bond et al. 1996; Nuss et al. 2000). This latter phenomenon has received considerable attention, and debate still continues on its underlying mechanism (see Ralph et al. 2000 for a review). In the South American case we are interested in the full evolution of the low (including, but not restricted to, its demise), given the prominence of the surface pressure drop and the relevant weather changes during its development. Later in this paper we further compare coastal lows in South America with CTDs along the west coast of North America, and relate their structural differences to differences in the synoptic-scale forcing and the regional topography.

While previous efforts have documented basic aspects of CLs along the subtropical west coast of South America, they were limited in their findings because the resolution of the observational network is not sufficient to resolve key subsynoptic aspects. This paper addresses some of the remaining questions on this phenomenon, including the typical large-scale environment attending the life cycle of CLs, the mean amplitude and propagation speed of the surface pressure perturbation, its phase relationship with circulation and thermodynamic changes in the lower troposphere, and the offshore extent of the wind and pressure anomalies. To this effect we have used high-resolution surface data from a regional network, routine synoptic observations, reanalysis fields, and high-resolution satellite imagery. Although CLs are a year-round phenomenon, we have concentrated our analysis on wintertime episodes (May–Sep), when CLs are better defined and exert a more pronounced impact on regional weather (e.g., Rutllant and Garreaud 1995).

The paper is organized as follows. Datasets are presented in section 2, and the analysis technique is described in section 3. The mean large-scale circulation and cloudiness features during CLs are described in section 4. In section 5 we present regional-scale aspects of CLs based on surface station data. A conceptual model for the generation and propagation of CLs is proposed in section 6. In section 7 we include a discussion on the role of free versus forced propagation during coastal lows, along with a comparison of South American CLs and western North America CTDs. A summary of our main findings is presented in section 8.

2. Datasets

The primary data used in this study are surface observations from a research network of nine automatic weather stations along the coast and farther inland, be-

TABLE 1. Surface stations. Variables measured include pressure (p), air temperature (T), relative humidity (RH), wind speed and direction (**u**), and solar radiation (SR). Measurement interval is 15 min in all stations.

Station	Lat (°S)	Lon (°W)	Elev (m MSL)	Variables measured
Caldera	27.08	70.87	11	p, T, RH, **u**, SR
Huasco	28.47	71.25	30	p, T, RH, **u**, SR
Cruz Grande	29.45	71.32	30	p, T, RH, **u**,
El Tofo	29.50	71.00	780	p, T, RH, **u**,
Lengua de Vaca	30.25	71.63	7	p, T, RH, **u**, SR
Los Molles	32.25	71.51	37	p, T, RH, **u**, SR
Las Cruces	33.50	71.62	26	p, **u**, SR
Lo Prado	33.45	70.93	1065	T, RH, **u**, SR

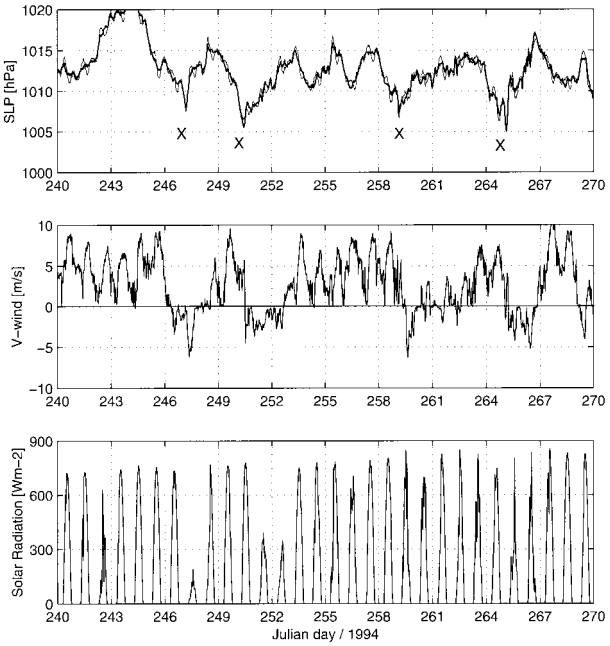

FIG. 3. (upper) The 30-min average of surface pressure, (middle) meridional wind, and (lower) solar radiation at station Lengua de Vaca (30.1°S, 71.5°W, 7 m MSL) from 27 Aug to 26 Sep 1994. In the upper panel, thin line is the observed surface pressure and thick line is the surface pressure with the mean diurnal cycle removed (anomaly filter). Crosses indicate selected coastal lows in this period (see text for further details).

tween 27°S and 34°S at an average alongshore spacing of 100 km (Fuenzalida and Rutllant 1995). Their locations are shown in Fig. 2 and their characteristics are summarized in Table 1. The network operated between November 1993 and November 1994, recording 30-min averages of pressure, air temperature, relative humidity, solar radiation at 2 m above ground, and wind vectors at 4 m above ground. Station Lengua de Vaca (30.3°S, 71.6°W, 7 m MSL) has a longer record, operating since 1991 in a near-continuous fashion. Synoptic reports every 3 h at San Felix Island [27.2°S, 80°W, 12 m above mean sea level (MSL) about 900 km off the coast] and Carriel Sur (36.8°S, 73.1°W, 21 m MSL) were used to extend our regional analysis to the open subtropical ocean and farther south.

The surface pressure at subtropical latitudes exhibits a pronounced mean diurnal march (diurnal and semidiurnal harmonics) produced by atmospheric tides. Over our target region, the amplitude of the mean diurnal cycle can be as large as 3 hPa (e.g., Fuenzalida 1995), masking pressure changes associated with CLs or other synoptic phenomena. In our subsequent analysis we removed the seasonal mean diurnal cycle from the original series using an anomaly filter. This filter was also applied to the series of air temperature, humidity, and wind components to remove the mean diurnal cycle produced by the daytime heating/nighttime cooling at the coast.

The large-scale tropospheric circulation was characterized using the pressure-level National Centers for Environmental Prediction–National Center for Atmospheric Research (NCEP–NCAR) reanalysis fields, described in detail in Kalnay et al. (1996). The original fields have a 6-h resolution on a 2.5° latitude–longitude grid and include all mandatory levels from 1000 to 100 hPa. One must keep in mind the coarse horizontal spacing of the reanalysis data compared with the relevant topographic features (e.g., half-width of the Andes Cordillera). We also used NCEP–NCAR reanalysis profiles of temperature in the original sigma levels (same horizontal and time resolution as the pressure-level fields) with 10 points below 700 hPa. Hence, the sigma-level profiles are able to capture the essential features of the lower troposphere over the coastal region (e.g., Garreaud et al. 2001). Preliminary analysis of low-level cloudiness was also possible on the basis of *Geostationary Operational Environmental Satellite-7* reduced resolution radiance [the International Satellite Cloud Climatology Project (ISCCP) B3 product (see Schiffer and Rossow 1985 for details)]. Here, we converted the original pixel maps at 2100 UTC (1800 local time) of visible radiance (0.6 μm) to a regular 0.5° × 0.5° latitude–longitude grid of albedo following the procedure described in Garreaud and Wallace (1997).

3. Case selection and compositing technique

The mean structure of coastal lows is investigated here using a compositing analysis of events selected on the basis of surface pressure minima at Lengua de Vaca (LdV), as described below. The station was selected because of the temporal coverage of their observations and its location on the coast of north-central Chile. A pressure minimum at LdV (in a temporal sense) is not necessarily the lowest pressure along the coast (in a spatial sense), but a composite based on these events produces a consistent signal of the coastal low evolution. Furthermore, as it will be shown later, most events selected in LdV were also recorded in the rest of the stations, so that our compositing analysis emphasizes the typical features of the CLs that affect the entire

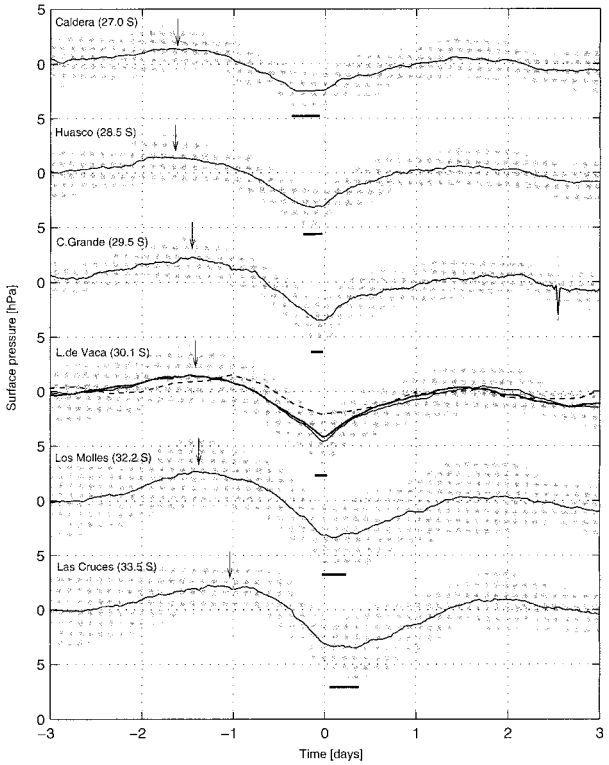

FIG. 4. Composite traces of surface pressure (solid line, hPa) at six stations along the coast of Chile (station name and latitude is indicated at the top of the corresponding trace) based on 21 CL episodes during 1994. Composite trace based on 57 episodes during 1991, 1993, and 1994 is also shown for the observed pressure at station Lengua de Vaca (thick line) and reanalyzed surface pressure at 30.0°S, 72.5°W (thick, dashed line). The mean diurnal cycle was removed at each station using an anomaly filter. The shaded area corresponds to the mean value plus and minus one standard deviation. Vertical arrows indicate the onset of the troughing; horizontal bars indicate coastal low culmination.

subtropical west coast of South America. Structural differences in the CL due to the selection method (e.g., key station for case identification) will be discussed elsewhere. Given the availability of other data we restricted our case selection to the austral winter (May–Sep) of 1991, 1993, and 1994. Figure 3 shows the time series of the surface pressure anomaly (diurnal cycle subtracted, p_s^*) at LdV for June–August 1994. The pressure is dominated by rapid fluctuations (2–3 days) with amplitudes of about 2.0 hPa, superimposed on synoptic fluctuations (7–10 days) with amplitudes of about 5 hPa.

A first pool of events was obtained by searching local minimum of p_s^* within a moving 5-day time window, and selecting those cases associated with a 24-h pressure drop in excess of 5 hPa. As an example, several local minima are readily identified during September of 1994 as shown in Fig. 3. Pronounced p_s^* minima can be caused by either midlatitude frontal disturbances approaching the coast or coastal lows. To separate these two conditions we used the wind speed and wind direction at LdV: frontal disturbances lead to north-northwesterly flow prior to the pressure minimum, while strong southerly winds precede a CL culmination followed by an alongshore wind relaxation. Thus, a minimum of p_s^* that satisfied the previous two conditions was classified as a *coastal low culmination* only if southerly winds (wind direction between 140 and 235°) in excess of 5 m s^{-1} prevailed at least during the 24-h prior to the p_s^* minimum. This last criterion eliminates about one-third of the original p_s^* minima, mostly prefrontal conditions (Rutllant and Garreaud 1995). For instance, the pressure minima on days 254 and 257 in Fig. 3 did not satisfy the wind criterion, and as such, they were not selected as coastal lows.

Application of this procedure yields a total pool of 57 CL culminations, nearly one event per week. We then took the traces of p_s^* and other station-based variables on a 6-day window centered at the culmination time (hour 0) of each case and averaged them to produce composite time series. Negative (positive) times refer to hours before (after) the culmination time. In the case of the NCEP–NCAR reanalysis, available at 0000, 0600, 1200, and 1800 UTC, culmination time was approximated by the nearest of the four. For solar radiation and albedo, day 0 was defined as the same day of the culmination if culmination time was before local noon. Otherwise, it would be the next day. Statistical significance of the composite anomalies was locally tested using a two-tailed Student's t-test at the 95% confidence level.

Figure 4 shows the composite trace of p_s^* at LdV using the 57 episodes identified during the austral winters of 1991, 1993, and 1994, as well as the composite based in the 21 cases in the winter of 1994. The similarity between the two traces of p_s^* at LdV is indicative that the number of events incorporated in the second composite is enough to ensure that the signal stands well above the sampling variability. Later, in section 5a, the composite traces of p_s^* at LdV and other coastal stations are described in detail. For the moment, it suffices to point out the key features of a CL: weak initial ridging, a marked drop down to the pressure minimum (CL culmination), and a more gradual recovery to the wintertime average value. To assess the ability of the reanalysis to mimic sea level pressure (SLP) changes at the coastline, Fig. 4 also shows the composite trace of reanalyzed p_s^* at the grid point (30°S, 72.5°W) closest to LdV. The reanalysis does capture the overall SLP evolution during the composite coastal low, but with an amplitude of just half of that observed in LdV.

4. Large-scale patterns

The composite mid- and upper-level circulation during a CL life cycle is characterized by a midlatitude ridge, drifting westward from the southern Pacific (Fig. 5). The ridge axis has a meridional orientation and it crosses the Andes almost simultaneously with the CL culmination at LdV. At this time, the geopotential gra-

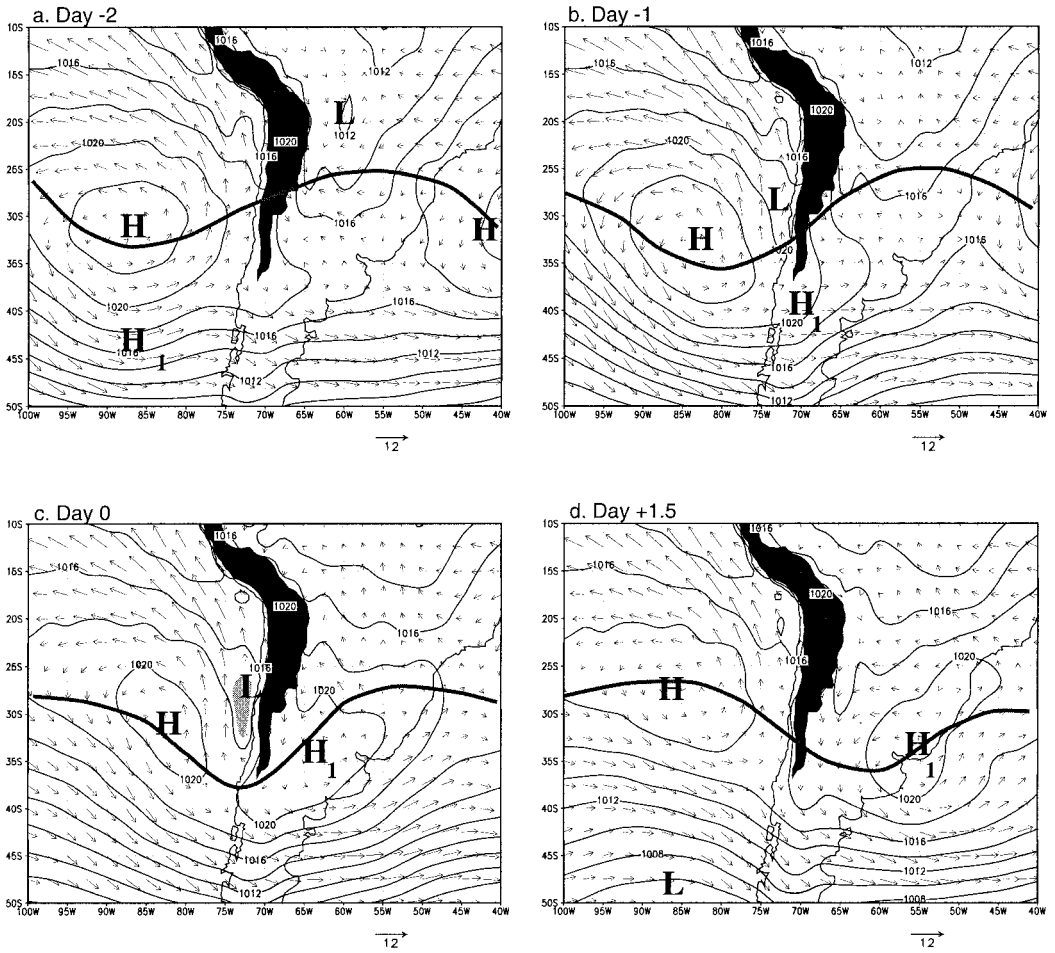

FIG. 5. Composite sea level pressure (contoured every 2 hPa) and 1000 hPa winds (arrows) at days (a) −2, (b) −1, (c) 0, and (d) +1.5. Thick, solid line is the 5680-m geopotential height at 500 hPa. Reference wind vector (in m s^{-1}) is shown at the bottom of each panel. Black area indicates terrain elevation in excess of 2000 m. High and low centers indicated by a letter H or L, respectively. H_1 indicates the center of the migratory anticyclone. For day 0 the light shading indicates SLP less than 1016.5 hPa.

dient is at a minimum over north-central Chile leading to significantly weaker than normal (by a factor 0.7) westerly flow through the middle and upper troposphere. Further, weak easterly winds ($|u| \leq 5$ m s^{-1}) over the subtropical Andes (~500 hPa) were found prior to or at the CL culmination in 35% of the cases, in connection with a northwest–southeast-oriented ridge. Midtropospheric subsidence downstream of the ridge axis contributed to the warming (1°C day^{-1}) and drying (1 g kg^{-1} day^{-1}) observed below 700 hPa to the west of the subtropical Andes from about 48 h before CL culmination. The nearly out-of-phase geopotential height anomalies between the middle and lower troposphere are better seen in the time–pressure section at 30°S, 72.5°W (Fig. 6), emphasizing the nonmidlatitude character of the coastal lows. Also notice that the 850-hPa surface remains level at about 1500 from day −1 to day +2.

Composite maps of SLP and 1000-hPa winds are shown for selected times in Fig. 5. Two days before CL culmination the surface conditions are close to climatology (cf. Fig. 1), but for a region of higher pressure around 40°S (noted by H_1 in Fig. 5) drifting just to the east of the midlevel ridge (thick solid line in Fig. 5). By day −1, the migratory surface ridge (H_1) has reached the coast of southern South America resulting in a stretching of the subtropical anticyclone eastward into the continent (recall that to the south of 38°S the elevation of the Andes drops to less than 1200 m). Simultaneously, a narrow surface trough develops between the subtropical anticyclone and the Andes Cordillera. Isallobaric analysis (not shown) indicates that at the time of the pressure minimum at LdV (day 0) the coastal trough has deepened and the localized region of negative pressure tendency has progressed down to 35°S (Fig. 5c). In spite of the coarse resolution of the reanalysis grid, the composite SLP field exhibits a closed coastal low centered at 30°S. Meanwhile the

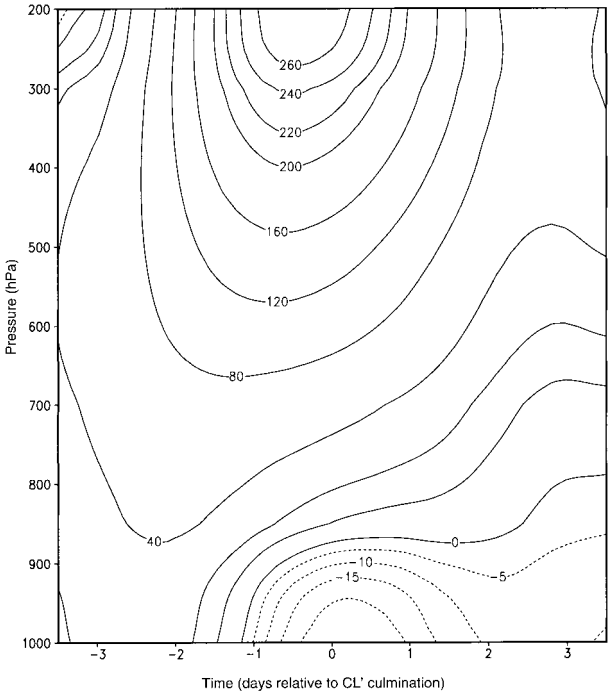

FIG. 6. Time–pressure section of the geopotential height anomaly (gpm, reanalyzed values) over the grid box centered at 32.5°S, 70°W. The anomalies were calculated at each level as the difference between the composite value and the long-term mean wintertime value. Time is relative to the coastal low culmination (day 0).

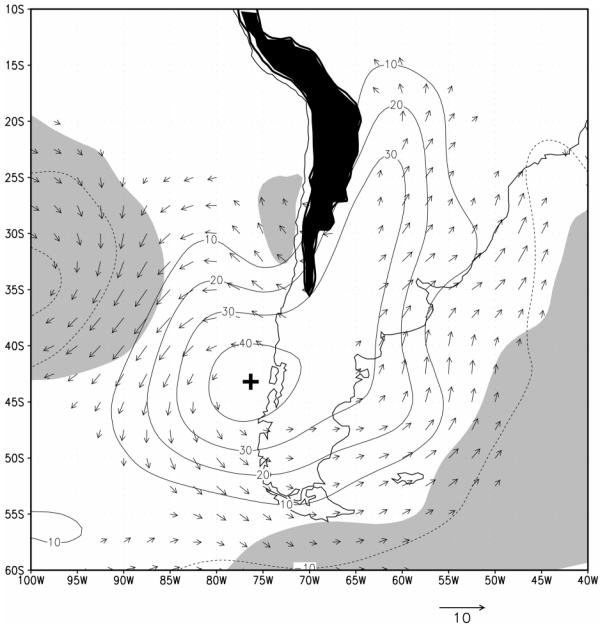

FIG. 7. Composite 925-hPa geopotential (contour) and wind (arrows) anomalies at culmination time (day 0). Contour interval is 10 m, negative values in dashed line, and the zero contour is omitted. Reference wind vector at the bottom of the figure is 10 m s^{-1}. Light shading indicates *negative* SLP anomalies larger than −1.5 hPa. Black area indicates terrain elevation in excess of 2000 m.

subtropical high has reached its maximum southeastward extension and the migratory anticyclone to the east of the Andes has moved northeastward. This distinctive high–low–high SLP pattern[1] and associated upper-air pattern at subtropical latitudes has been earlier identified in synoptic studies on coastal lows in north-central Chile (e.g., Rutllant and Garreaud 1995). By day +1.5, the trough has vanished from the coast as an extratropical depression (noted by the L in Fig. 5), often accompanied by a cold front, has moved close to the coast of southern Chile, and the migratory anticyclone has slowly drifted into northern Argentina and southern Brazil.

At the 925-hPa level (near the base of the subsidence inversion), a wide area of positive height anomalies extends from 30° to 50°S off the western coast of South America and protrudes to the east of the subtropical Andes as far as 20°S (Fig. 7) in connection with the migratory low-level ridge. The positive height anomaly exhibits a conspicuous trough just off the coast of north-central Chile, coincident with a region of negative SLP anomalies (25°–35°S) that signals the CL. The *anomaly* trough suggests cross-shore and alongshore scales of 500 and 1000 km, respectively, for the CL at the mature stage. At the same level, wind anomalies are approximately in geostrophic balance with the height anomalies. Of particular interest is a wide area of easterly anomalies off the coast of central Chile, associated with a veering from the climatological onshore flow to offshore (easterly) flow before and at CL culmination. The veering is somehow difficult to notice in the composites of actual winds (Fig. 5) since the coastal winds within the MBL are dominated by the alongshore component.

The composite maps of albedo for days −1, 0, and +1, shown in Figs. 8a–c document changes in the cloud cover at the coast and over open ocean, providing independent support for the synoptic picture previously described. The extensive and highly persistent deck of stratocumulus off the subtropical west coast of South America (e.g., Klein and Hartmann 1993) is disrupted by a region of clear skies (low albedo) that expand offshore over time before the CL culmination (Figs. 8a, b). Similar marine stratocumulus clearing episodes are observed along the coast of California, associated with offshore flow effects (Kloesel 1992). At day 0 the region of clear skies reaches its maximum extension, collocated with the coastal low (c.f. Figs 5c–8a). The clear skies are likely indicative of a shrinking of the MBL, but the lack of upper-air data off the coast prevents a more thoughtful diagnosis of the clearing. The clear-sky region begins to vanish by day +1, as a poleward-moving wedge of stratus returns along the coast, sometimes

[1] This pattern is remarkably similar to the synoptic configuration during cold air incursions to the east of the subtropical Andes (e.g., Marengo et al. 1997; Vera and Vigliarolo 2000; Garreaud 2000), suggesting simultaneous occurrence of coastal lows in central Chile and cold surges in southern Brazil and Bolivia.

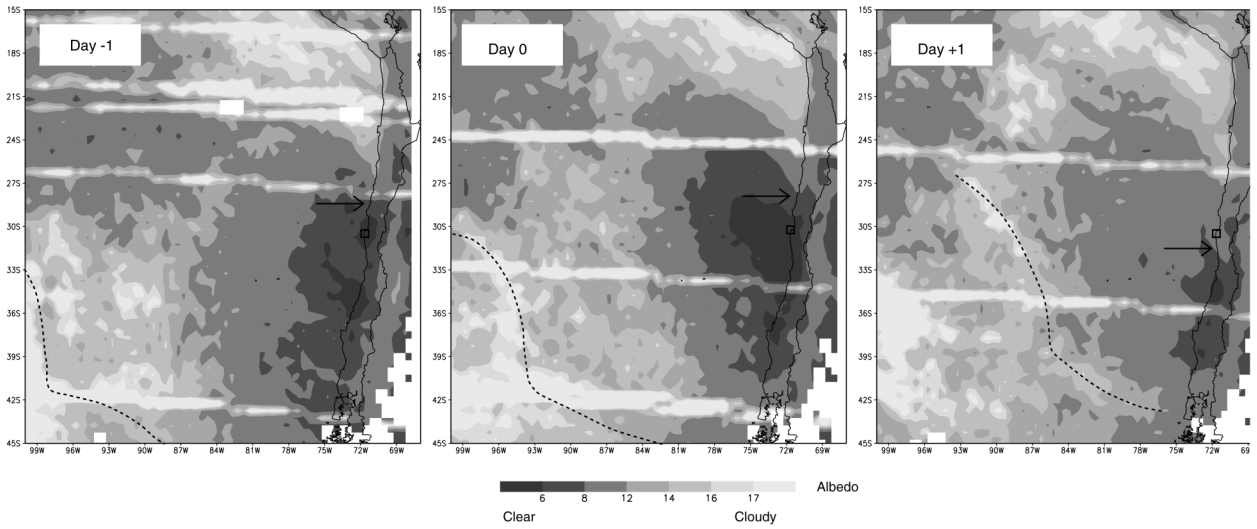

FIG. 8. Composite maps of albedo at day −1, 0, and +1. Arrows indicate leading edge of the stratocumulus deck along the coast. Small open square indicates position of station Lengua de Vaca (30°S). Dashed line indicates the approximate position of a frontal system at surface.

merging with midlevel cloudiness associated with the frontal system approaching southern Chile (Fig. 8c).

5. Regional aspects

a. Changes at sea level

Figure 4 shows traces of the surface pressure anomaly (p_s^*) in the six coastal stations at sea level between 27° and 33°S averaged for the 21 CL episodes identified in LdV during 1994. It is useful to remember that the composite procedure based on the culmination time in LdV smears out the signal at the other stations due to variations in the episode's propagation speed. The composite traces exhibit an asymmetric V shape, with a lifespan of about 3 days and amplitude increasing poleward from 3.5 to 6.1 hPa. In all stations, the surface pressure begins gradually to increase about 2.5 days before the CL culmination at LdV, reaching a significant positive anomaly during day −1, followed by a pronounced pressure drop down to the minimum. After culmination, the pressure recovers to its mean wintertime value in about a day without reaching significant positive anomalies. The same data in Fig. 4 can be used to construct alongshore composites of p_s^* traces at different times (not shown). At day 0, the composite CL appears as a closed low with a surface pressure minimum around LdV (30°S) flanked at both sides by an alongshore pressure gradient of about 0.3 hPa (100 km)$^{-1}$, as previously suggested by the reanalysis data.

A weaker, lagged evolution is found in the composite traces of p_s^* away from the coastal network (Fig. 9). At San Felix Island, weaker SLP maximum and minimum occur about 12 h later than their counterparts at LdV, while at Carriel Sur (inland mountains less than 1000 m) the initial ridging continues ~18 h after the beginning of the pressure drop at LdV. The nearly synchronous ridging–troughing sequence at these two stations is consistent with the large-scale pattern found in the previous section (i.e., ridge–trough couplet drifting eastward at midlatitudes). Thus, the developing stage of the CL at subtropical latitudes occurs as pressure *increases* farther south and away from the coast (synoptic-scale surface ridging), while the CL culmination occurs when pressure is decreasing elsewhere (synoptic-scale surface troughing). The more rapid and pronounced pressure fall and rise along the coast farther north indicates that the basic large-scale changes are time shifted and amplified along the subtropical coast. This presumably represents the local impact of the coastal low.

Figure 4 also reveals the southward propagation of some composite features at a mean speed that can be estimated from a least squares fit of the station data. The initial decrease of surface pressure (i.e., the first time in the composite trace at which $\partial p_s^*/\partial t < 0$, indicated by an arrow in Fig. 4) propagates at $C_i = 28.4 \pm 5.6$ m s^{-1}, although inspection of individual CLs reveals a number of cases in which the onset of the troughing occurs nearly simultaneously along the coastal network (27°–33°S). The pressure minimum that signals the local culmination time (indicated by a bar in Fig. 4) propagates slower and more regularly, at a mean speed $C_c = 16.1 \pm 4.9$ m s^{-1}. Furthermore, a southward propagation of the p_s^* minimum was found in 18 out of 21 CLs, although with significant dispersion in the regional value of C_c (10–30 m s^{-1}). The mean value of C_c is consistent with previous estimates based on synoptic data (Rutllant and Garreaud 1995).

A marked change in the coastal surface winds is observed during the CL lifespan, as shown in Fig. 10a by the composite traces of wind speed and the dominant

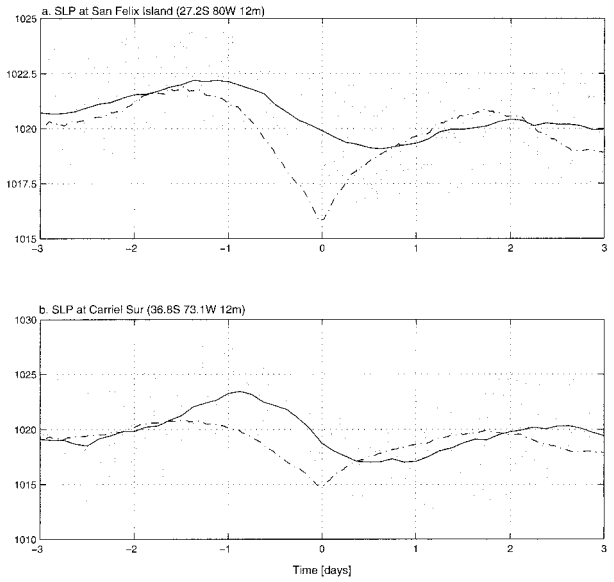

FIG. 9. (a) Composite trace of surface pressure (solid line, hPa) at San Felix Island (27.2°S, 80°W 12 m MSL). The shaded area corresponds to the mean value plus and minus one standard deviation. The wintertime mean diurnal cycle has been removed from the observed time serie (3-h average) using an anomaly filter. For reference, the composite trace of surface pressure at Lengua de Vaca is shown by the dot–dashed line. Time is centered in the hour of minimum pressure at Lengua de Vaca. (b) As in (a) but for station Carriel Sur (36.8°S, 71.6°W, 21 m MSL).

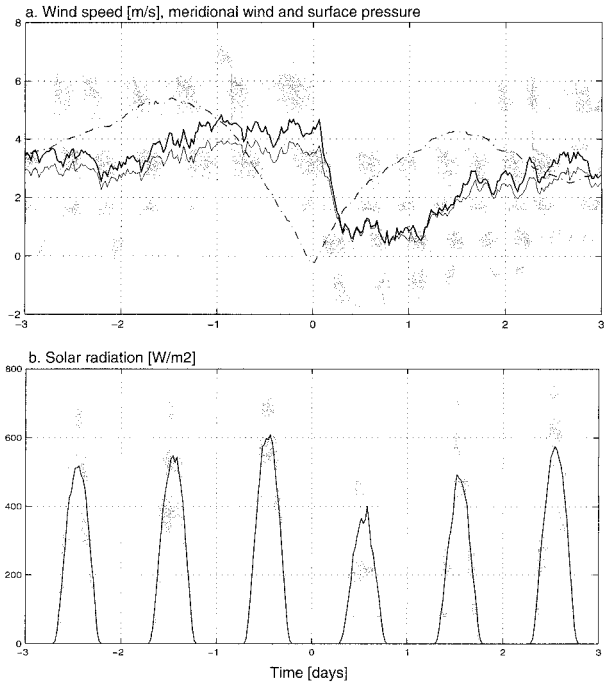

FIG. 10. (a) Composite wind speed (thick line, m s^{-1}) and meridional wind (thin line) at Lengua de Vaca (30.3°S, 71.6°W, 7 m MSL). The shaded area corresponds to the mean speed plus and minus one standard deviation. The wintertime mean diurnal cycle has been removed from the observed time series (3-h average) using an anomaly filter. For reference, the composite trace of surface pressure at Lengua de Vaca is shown by the dot–dashed line. Time is centered in the hour of minimum pressure at Lengua de Vaca. (b) Composite solar radiation (W m^{-2}) at Lengua de Vaca. The shaded area corresponds to the mean speed plus and minus one standard deviation.

meridional wind component (roughly alongshore) at LdV. About 2 days before the p_s^* minimum, the southerly wind increases gradually to reach a maximum over 5 m s^{-1} just at the culmination time, followed by a sharp decrease down to ~1 m s^{-1}. Isallobaric wind estimates are in agreement with the observed southerly acceleration (Rutllant 1994, 1997). The weak southerlies persist for about a day, and sometimes the wind reverses to weak northerlies along the coast. Pilot balloon observations at LdV during intensive field experiments reveal that the strong surface southerlies before the CL culmination are associated with an alongshore low-level jet at about 150–200 m above the surface, and lead to an almost simultaneous decrease of SST along the coast due to enhanced coastal upwelling around 30°S (Rutllant 1993, 1997). A transition from enhanced to relaxed southerlies is also observed, at varying degrees, at the rest of the coastal stations within 4 h from the local culmination (not shown).

A transition from sunny to overcast conditions, roughly centered at the culmination time, is also evident in the composite solar radiation at LdV (Fig. 10b), as well as the other coastal stations. These results are in agreement with the southward displacement of a wedge of coastal stratus observed in the composite maps of albedo (Fig. 8). The leading edge of the stratus has a cross-shore scale of ~150 km, and it moves southward at about 17 m s^{-1}, very close to the estimated propagation speed of the p_s^* minimum. In spite of the solar radiation signal, there are no significant changes in relative humidity and air temperature at sea level associated with the passage of a CL. Probably, enhanced cold air advection and colder SST (in connection with the strong southerlies) compensate for the increment of solar heating before the CL culmination.

b. Changes in the MBL and at the inversion level

The development of a CL along the subtropical coast is accompanied by a strengthening of the subsidence inversion and a descent of its base, frequently down to the surface, as documented in Rutllant (1981, 1983) using routine radiosonde data at Quintero (32.5°S, 71.3°W, 8 m MSL). To illustrate this behavior, we have used 1200 UTC (0800 local standard time) sigma-level NCEP–NCAR reanalysis profiles of potential temperature at 32.5°S, 72.5°W as a surrogate of the Quintero soundings. The composite profiles for the CL episodes identified between 1991 and 1994 are shown in Fig. 11. Two days before the minimum pressure at LdV, the profile is close to climatology (e.g., Rutllant 1994), with a well-mixed MBL below 950 hPa and the top of the temperature inversion at about 900 hPa. By day 0, there

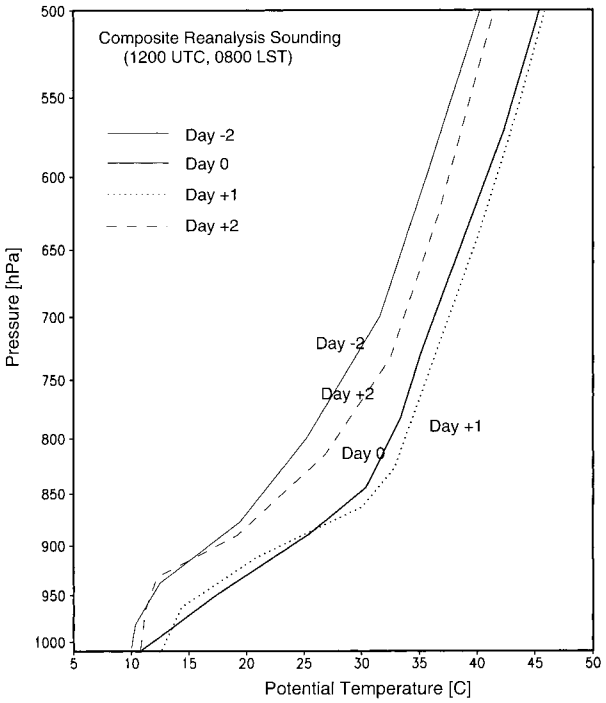

FIG. 11. Composite profiles of potential temperature (1200 UTC reanalysis values) over the grid box centered at 32.5°S, 72.5°W, for days −2, 0, +1, and +2.

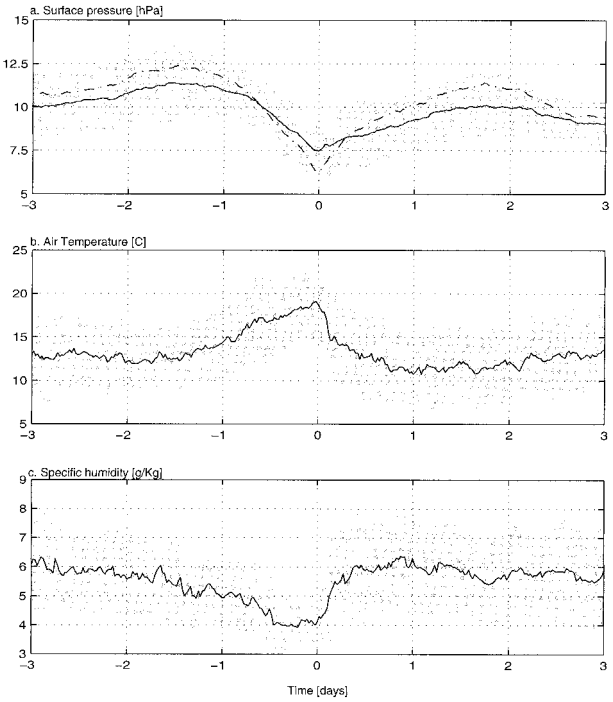

FIG. 12. (a) Composite trace of surface pressure (solid line, hPa) at El Tofo (29°S, 71°W, 780 m MSL). The wintertime mean diurnal cycle has been removed from the observed time series (30-min average) using an anomaly filter. The shaded area corresponds to the mean value plus and minus one standard deviation. For reference, the composite trace of surface pressure at Lengua de Vaca is shown by the dot–dashed line. (b) As in (a) but for the 2-m air temperature. (c) As in (a) but for 2-m specific humidity. In all panels time is in days, centered at the hour of minimum pressure at Lengua de Vaca.

is a generalized warming of the lower and middle troposphere. The largest warming (~6°C) occurs between 900 and 800 hPa. Of particular interest is the upward *and* downward expansion of the temperature inversion, so that, even in this composite, the MBL vanishes by day 0. One day later, the warming continues at midlevels, at the same time that the recovery of the MBL has begun. By day +2 the generalized cooling, in connection with the incoming midlatitude trough, has brought the profile to near-normal conditions (Fig. 11).

Further details on the timing and amplitude of the changes in the MBL/inversion layer can be obtained from the observations at the two elevated AWS within the regional network. Station El Tofo is located at 780 m MSL, close to the climatological *base* of the subsidence inversion over this region (Schemenauer et al. 1988). The composite trace of p_s^* at El Tofo parallels its counterpart at LdV (about 120 km to the south), although its amplitude is about 70% of that observed at sea level (Fig. 12a). Note that this signal in pressure is produced by changes occurring above the top of the MBL, stressing the prominent role of the synoptic scale in setting the poleward pressure gradient. A gradual warming–drying starting 30 h before the culmination of the CL is terminated by a sharp cooling–moistening within 6 h after the pressure minimum (Figs. 12b,c). This marked asymmetry in the rate of warming and cooling is evident in nearly all individual episodes. Air temperature continues a more gentle decrease during day +1, down to a minimum about 2°C lower than the pre-CL value. The evolution of temperature and moisture, along with the composite soundings shown in Fig. 11, is indicative of a gradual strengthening and descent of the subsidence inversion before the p_s^* minimum, followed by a rapid recovery of the MBL immediately after culmination time.

Station Lo Prado is located on a saddle point of the coastal range where the zonal component of the wind is dominant, at 1000-m elevation and near the climatological *top* of the inversion layer at 33°S (Rutllant and Garreaud 1995). The gradual warming–cooling sequence is symmetrical with respect to the culmination time at the closest coastal station, Las Cruces, (Figs. 13b,c). The temperature increment at the inversion top has a similar magnitude (~+5°C) to that observed at the inversion base (El Tofo composite). Sustained easterly winds begin simultaneously with the drop of surface pressure at LdV, and thus they lead the beginning of the local warming by about 12 h (Fig. 13a). The easterly wind increases up to nearly 10 m s^{-1}, followed by a sharp transition to weak westerlies around the culmination time at LdV. The simultaneous changes of zonal wind at Lo Prado and surface pressure at LdV are noteworthy considering the 380-km spacing between the two stations. In some cases, the westerly flow and the in-

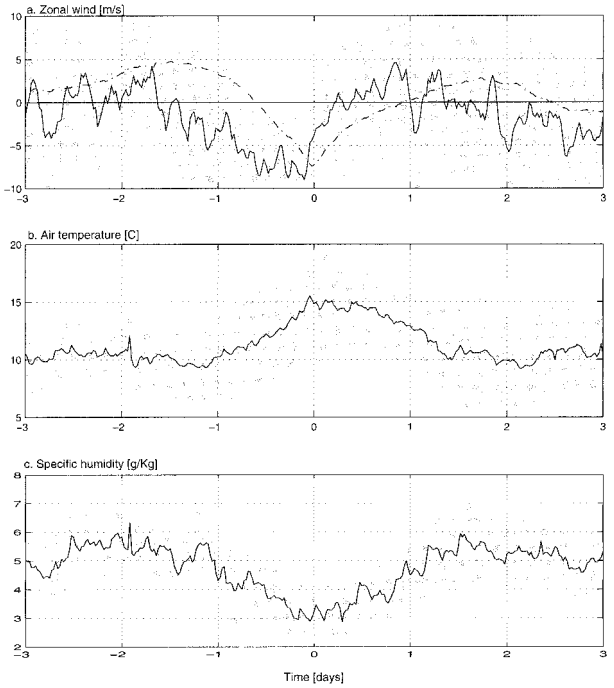

FIG. 13. (a) Composite trace of zonal wind (solid line, hPa) at Lo Prado (33.5°S, 70.9°W, 1065 m MSL). The wintertime mean diurnal cycle has been removed from the observed time series (30-min average) using an anomaly filter. The shaded area corresponds to the mean value plus and minus one standard deviation. For reference, the composite trace of surface pressure at Lengua de Vaca is shown by the dot–dashed line. (b) As in (a) but for the 2-m air temperature. (c) As in (a) but for 2-m specific humidity. In all panels time is in days, centered at the hour of minimum pressure at Lengua de Vaca.

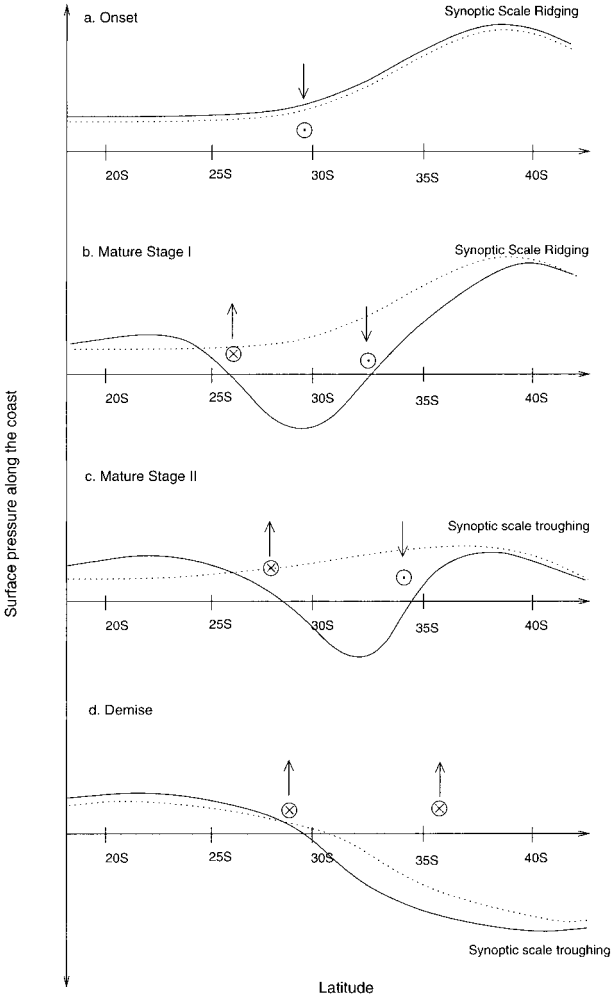

FIG. 14. Schematic representation of the surface pressure profile along the west coast of South America during the evolution of a coastal low. At each stage, the actual profile along the coast is shown in a solid line and the large-scale synoptic profile (unaffected by the topography) is shown in a dashed line. Dotted (crossed) circles indicate offshore (onshore) low-level winds, in geostrophic balance with the coastal meridional pressure gradient. Vertical arrows indicate the direction of the topographically induced vertical motion required to satisfy mass continuity close to the mountainous coastline.

version rise after the CL culmination are strong producing advection of cool, moist marine air into the inland valleys to the east of the coastal range. Notice that the stronger westerly flow at Lo Prado lags the SLP minimum at LdV by about 6 h, consistent with the previously estimated propagation speed of 17 m s^{-1}.

6. Conceptual model

By merging the results from the synoptic and regional analysis, a conceptual model of the composite CL evolution is now proposed. The climatological equatorward surface pressure gradient along the subtropical west coast of South America can be reversed when a migratory anticyclone (connected with the midlevel ridge) approaches southern Chile at about 40°S (Fig. 14a). The large-scale low-level wind, dominated by the southerly component, adjusts geostrophically to this change by veering from onshore to offshore (easterly) flow. The continuity requirement after the onset of the low-level easterlies off the coast seems to be satisfied by downslope flow over the western side of the Andes, so that marine, cool air begins to be replaced by adiabatically warmed air, as evidenced by the strengthening and downward expansion of the inversion layer. Recalling that the pressure remains nearly constant at ~1500 m MSL, the low-level warming leads to the hydrostatic fall in surface pressure. Downslope flow may be further enhanced when easterly flow exists in the middle troposphere, in connection with a northwest–southeast-oriented ridge, leading to foehn-like conditions.

The evolution of the alongshore surface pressure at the onset of a CL is then determined by two opposite effects whose magnitude varies with latitude: synoptic-scale ridging and topographic troughing. To the south of 38°S, the synoptic forcing is large and the height of the Andes is less than 1000 m MSL, so the surface pressure is largely dominated by the synoptic effect (e.g., pressure trace at Carriel Sur; Fig. 9). Between 25°

and 35°S, the synoptic forcing is weaker and the Andes top exceeds 4000 m MSL, so that the initial pressure rise (synoptically forced) is eventually offset by the topographic troughing marking the onset of the coastal low at subtropical latitudes (Fig. 14b). The simultaneous occurrence of sustained easterlies within the inversion layer and the beginning of the surface pressure drop at sea level lends support to this hypothesis (cf. Figs. 4 and 12). Farther to the north, the synoptic forcing is very weak, so neither the synoptic nor the topographic effects are important, and the stratus-topped MBL remains unperturbed.

The drop of surface pressure along the subtropical coast further increases the poleward pressure gradient between the developing CL and the midlatitude anticyclone, eventually decreasing the surface pressure (through adiabatic warming) to the south of the pressure minimum. At the same time, an equatorward pressure gradient and balanced westerly flow develop off the coast to the north of the coastal pressure minimum. Considering a representative height of the topographic barrier (coastal range and the Andes Cordillera) $h_m \sim 2000$ m and $U \sim 3$ m s^{-1} as the upstream onshore velocity scale, the Froude number [Fr $= U/(f \times h_m)$] evaluated at 27°S is Fr ~ 0.3. Thus, the onshore flow is likely blocked by the coastal range, locally deepening the MBL and forming a weak surface mesoridge at the northern coast. Unfortunately, this later feature is not documented in our analysis because the northernmost coastal station is at 27°S.

As the axis of the midlatitude anticyclone moves to the east of the Andes (southern Argentina) pressure begins to drop in southern Chile. Eventually the pressure gradient between the subtropics and midlatitudes becomes equatorward, and the large-scale coastal wind backs from offshore to onshore flow, marking the demise of the coastal low (Fig. 14d). At this time, there is a marked alongshore gradient of surface pressure between northern Chile (where the MBL has remained unperturbed or slightly deepened) and the subtropical latitudes (where the MBL is very low; see Fig. 11). The cessation of the subsiding offshore flow, however, does not imply the recovery of the surface pressure. Rather, the rise of the surface pressure at a given point along the coast will occur in concert with the local recovery of the cool MBL, as evidenced in the composite traces at El Tofo and LdV (Fig. 12). Yet, such a positive pressure tendency caused by the low-level cooling might be partially offset by the synoptic-scale approaching trough (mid- and upper-level divergence).

7. Discussion

The evidence presented in this paper suggests that the initial and mature stage of a coastal low (surface pressure decreasing along the subtropical coast) is largely produced by the interaction between the large-scale forcing (including changes above the MBL) and the topography, in the form described above. A rough estimate of the topographically induced subsidence over the subtropical coast can be obtained from a scale analysis of the continuity equation neglecting the alongshore variation of the meridional wind ($\partial u/\partial x + \partial w/\partial z = 0$) and assuming a wall-like mountain. Let $U \sim 3$ m s^{-1} be the low-level, quasigeostrophic offshore velocity scale (obtained from the reanalysis composite; Fig. 5); X the cross-shore scale at which u approaches asymptotically to U; W the vertical velocity scale; and $H \sim 2$ km the height scale of the layer where the most significant warming takes place. The Rossby radius of deformation X is an appropiate cross-shore scale, so $X = NH/f \sim 200$ km (where $N = 1.5 \times 10^{-2}$ s^{-1} is the reference Brunt–Väisälä frequency, and f, the Coriolis parameter, is evaluated at 30°S). The calculated scale for the vertical velocity results in $W \sim -3$ cm s^{-1}, nearly five times larger than the large-scale subsidence (reanalyzed value) ahead of the midlevel ridge. With this figure, we can estimate the adiabatic warming and the associated pressure fall by integrating the hydrostatic equation over the lower troposphere:

$$\Delta T_{\text{adb}} = \frac{T_0}{g} WN^2 \approx 6 \text{ K day}^{-1} \quad (1)$$

$$\Delta p_h = -\frac{gp_0}{RT_0^2} \Delta T_{\text{adb}} H \approx 5 \text{ hPa day}^{-1}, \quad (2)$$

where $T_0 \sim 280$ K is the reference temperature of the lower troposphere and $p_0 \sim 1010$ hPa is a reference surface pressure. Thus, the topographic troughing becomes comparable to the synoptic-scale ridging in about a day. Such a drop in surface pressure would be more or less uniform along the subtropical west coast (25°–35°S), leading to a quasi-stationary development of the coastal low during the period of favorable synoptic-scale conditions (typically 2–4 days).

Once the synoptic-scale forcing ceases to be favorable for the development of the coastal low (low-level zonal flow backs from easterly to westerly), the pronounced equatorward pressure and MBL depth gradients along the coast are favorable for free waves to develop, trapped by the Coriolis force against the coastal and Andean topography. Recall that in the composite (Fig. 4), and in many individual cases, the recovery of the surface pressure (i.e., the initial time at which $\partial p_s^*/\partial t > 0$ after the pressure minimum) occurs at increasing times as one looks at the coastal stations from north to south, at a propagation speed $C_c \sim 16$ m s^{-1}, and is typically associated with a relaxation or reversal of the alongshore winds. Further, the high-resolution visible imagery (Figs. 8b,c) suggests that, in most cases, the recovery of the coastal stratocumulus occurs as a wedge (cross-shore scale ~200 km) moving from the north at a propagation speed close to C_c.

Topographic Rossby waves (e.g., Skamarock et al. 1999) will indeed move the coastal pressure minimum

to the south.[2] This displacement is, however, too slow ($C_R \sim 6$ m s^{-1}) compared with the observations, and hence, it is unlikely that topographic Rossby waves play a significant role during the demise of the coastal low. Bores and trapped gravity currents can produce pressure, wind, and cloudiness signatures similar to those observed after the culmination of the coastal low, but the northerly winds after the surface pressure minimum are too slow compared with the observed propagation speed. A third candidate to explain the recovery of the MBL/surface pressure is a trapped Kelvin wave. The predicted phase speed for a Kelvin wave in which the MBL and the capping inversion behave as one layer (e.g., Fig. 11) is given by $C_K = [g^*(H + H_1)]^{1/2}$, where g^* is the reduced gravity, H the depth of the unperturbed MBL, and H_1 the thickness of the unperturbed inversion (e.g., Ralph et al. 2000). Using typical values for subtropical South America ($g^* \sim g/40$, $H \sim 600$ m, $H_1 \sim 600$ m) results in $C_K = 17$ m s^{-1}. This rough agreement, together with the wind and cloudiness changes around the time of surface pressure minimum, suggests that the recovery of the MBL after the culmination of the coastal low might occur as a Kelvin wave (see also Rutllant 1994). Nevertheless, we do not have enough data to conclusively answer whether or not the propagation is a Kelvin wave. Key data missing include continuous profiles of temperature and humidity at several points along the coast in order to define the shape of the MBL leading edge. Mesoscale modeling efforts are currently underway to clarify this point.

At this point it is interesting to compare the mean structure of CTDs along the west coast of South and North America. The structure and dynamics of CTDs in this latter region have received considerable attention, as recently reviewed by Nuss et al. (2000). The existence of similar CTDs in these regions is expected, given the broad similarities in regional topography, oceanic boundary conditions, and mean atmospheric circulation. Further, low-level, localized offshore flow in the lower troposphere also appears as a robust feature in the early stages of warm-season CTDs along the west coast of North America (Mass and Bond 1996), and idealized numerical simulations over this region show that offshore flow can lead to adiabatic warming and evacuation of the MBL near the coast causing the formation of a surface mesolow (Skamarock et al. 1999). The wind shift that characterize CTDs along the coast of central and northern California tends to occur 3–4 h after a relatively small surface pressure minimum (less than 1 hPa with respect to undisturbed conditions), and it is followed by a gradual and more prominent pressure rise (~2–3 hPa) in the next 3–12 h. Thus, while the amplitude and qualitative evolution of the surface pressure anomalies during the full cycle of a North American CTD are similar to their South American counterparts, the strength of the precursor coastal low and the subsequent coastal ridge are inverted (recall that positive SLP anomalies after the culmination are not significant in the composite South American CL; Fig. 4). This asymmetry in the surface pressure anomalies during the life cycle of a coastally trapped disturbance is the basis for its generic name: coastal low along the west coast of South America and South Africa, and coastal ridges along the west coast of North America and Australia (Reason and Steyn 1990).

We hypothesize that the more prominent troughing in CTDs in the subtropical west coast of South America is related with the sharper and higher near-coastal topography (including the Andes Cordillera) along this region, which implies stronger vertical velocities (and, hence, adiabatic warming) than in North America given the same low-level offshore flow. The topographically enhanced adiabatic warming during CLs might also explain the differences in the vertical structure of North and South American CTDs. In the former case, Ralph et al. (1998, 2000) document a significant upward expansion of the MBL inversion after the surface wind shift but rather minor changes in the MBL depth. In our composite, in addition to the warming at and above the levels of the trade inversion, there is a clear shrinking of the MBL as the surface pressure drops, with the inversion base reaching the surface in many individual CLs (see Fig. 11).

Another common feature of CTDs in North and South America is their poleward propagation. Along the western coast of North America, the wind shift, the precursor coastal low, and the subsequent coastal ridge tend to move in concert at a ground-relative speed between 7 and 12 m s^{-1}. In many cases, the wind shift stalls during daytime, leading to its decoupling with the coastal low. For a typical episode in North America, Ralph et al. (2000) found that its propagation speed and structure ''is best characterized as a mixed Kelvin wave–bore propagating within the inversion above the MBL, with the MBL acting as a rigid lower boundary.'' In our composite along the west coast of South America the minimum pressure (coincident with the recovery of the MBL) moves poleward faster, at about 16 m s^{-1} ground relative speed (~18 m s^{-1} intrinsic phase speed), within the range of speeds for Kelvin wave when both the MBL and the MBL inversion behave as one layer (Fig. 11).

The alongshore wind anomalies during the South American coastal lows are similar but weaker ($\Delta v \sim 4$ m s^{-1}) than those observed in North America ($\Delta v \sim 8$ m s^{-1}). In some episodes we did observe a transition from the climatological southerly winds to the fully disturbed northerly winds. Nevertheless, our wind observations come from surface land stations (in contrast with coastal buoys in North America), likely influenced by the local topography, so we cannot confidently assess

[2] Using linear theory, Rynes (1970) provides the alongshore phase speed of a topographic Rossby wave: $C_R = \alpha N/(k^2 + l^2)^{1/2}$, where α is the mountain slope, and k and l are the cross- and alongslope wavenumbers, respectively. Using $\alpha = H/X = 2$ km/200 km, and a nominal wavelength $L_x = L_y \sim 500$ km, yields $C_R \sim 6$ m s^{-1}.

the changes in coastal wind during CL episodes. For this reason we have also refrained from assessing any diurnal cycle in the wind shift along the subtropical west coast of South America (a prominent feature in North American CTDs). Yet, the surface pressure observations, after subtracting the diurnal cycle, do not indicate any preferential timing for the onset, culmination, or demise of the CL.

8. Concluding remarks

Coastal lows on the west coast of subtropical South America are observed to occur year-round at a rate of about one per week, causing significant day-to-day weather changes along the coast and further inland, especially during the austral winter. Their mean structure and evolution has been documented in this work on the basis of atmospheric reanalysis, visible satellite imagery, and surface observations from a regional network along the coast of north-central Chile.

The large-scale synoptic environment during the CL development stage is characterized by a midlatitude surface anticyclone drifting from west to east connected with a midlevel ridge. The low-level anticyclone seems instrumental in the onset and deepening of the CL at subtropical latitudes because it can revert the alongshore pressure gradient leading to offshore flow along the coast. The easterly winds and enhanced subsidence along the subtropical coast (25°–35°S) enhance the trade inversion *and* depress the MBL. Since pressure remains nearly constant at about 1500 m MSL, the replacement of cold, marine air by adiabatically warmed air produces a surface coastal low that extends about 500 km away from the coast. Consistently, clear skies and warm, dry conditions prevail at the coast during the developing stage of the CL. This stage is also characterized by an intensification of the upwelling-favorable southerly winds along the coast. The surface pressure at subtropical latitudes reaches the local minimum (CL culmination) as the axis of the midlatitude, midlevel ridge axis crosses the Andes Mountains.

The demise of the CL (surface pressure rising) tends to occur as a midlatitude surface-low/upper-trough approaches southern Chile. In this condition the coastal flow reverts from offshore to onshore and the adiabatic warming ceases to act. The recovery of the surface pressure toward mean values occurs at increasing times as one looks at the coastal stations from north to south (mean propagation speed $C_c \sim 16\ \mathrm{m\ s^{-1}}$) and is typically associated with a relaxation or reversal of the alongshore winds and the reestablishment of the cloud-topped MBL. Thus, the demise stage of the coastal low resembles a trapped Kelvin wave propagating along the coast from northern Chile (where the MBL was not perturbed or even thickened) into subtropical latitudes in about a day or so.

Acknowledgments. This research was supported by FONDECYT (Chile) under Grant 1000913, and by the Department of Research and Development, Universidad de Chile, under Grant I99/002. The regional network in north-central Chile was also supported by FONDECYT under Grant 1930806. Rodrigo Sanchez assembled data from this network. NCAR–NCEP reanalysis was provided by NOAA's Climate Diagnostics Center. The B3 ISCCP data were obtained from the NASA-Langley Research Center EOSDIS Distributed Active Archive Center. The authors gratefully acknowledge P. Aceituno for comments and a careful reading of the manuscript. Constructive criticisms and thoughtful comments of two anonymous reviewers were highly appreciated.

REFERENCES

Bond, N., C. Mass, and J. Overland, 1996: Coastally trapped southerly transitions along the U.S. west coast during the warm season. Part I: Climatology and temporal evolution. *Mon. Wea. Rev.*, **124,** 430–445.

Dorman, C. E., 1985: Evidence of Kelvin waves in California's marine layer and related eddy generation. *Mon. Wea. Rev.*, **113,** 827–839.

Fuenzalida, H., 1995: Daily cycle of sea level atmospheric pressure around 30°S along the Chilean coast. *Contrib. Atmos. Phys.*, **69,** 349–353.

——, and J. Rutllant, 1995: Coastal lows in north-central Chile: An observational study. Informe Final Proyecto FONDECYT No. 0502-94, 39 pp.

——, ——, and J. Vergara, 1990: Estudio de los estratocúmulos costeros y su potencial como recurso hídrico (II Parte). Informe Final Proyecto FONDECYT No. 0511-88, 31 pp.

Garreaud, R. D., 2000: Cold air incursions over subtropical South America: Mean structure and dynamics. *Mon. Wea. Rev.*, **128,** 2544–2559.

——, and J. M. Wallace, 1997: The diurnal march of the convective cloudiness over the Americas. *Mon. Wea. Rev.*, **125,** 3157–3171.

——, J. Rutllant, J. Quintana, J. Carrasco, and P. Minnis, 2001: CIMAR-5: A snapshot of the lower troposphere over the subtropical southeast Pacific. *Bull. Amer. Meteor. Soc.*, **82,** 2193–2207.

Gill, A. E., 1982: *Atmosphere–Ocean Dynamics.* Academic Press, 662 pp.

Kalnay, E., and Coauthors, 1996: The NCEP/NCAR 40-Year Reanalysis Project. *Bull. Amer. Meteor. Soc.*, **77,** 437–471.

Klein, S. A., and D. L. Hartmann, 1993: The seasonal cycle of low stratiform clouds. *J. Climate,* **6,** 1587–1606.

Kloesel, K. A., 1992: Marine stratocumulus clearing episodes observed during FIRE. *Mon. Wea. Rev.*, **120,** 565–578.

Marengo, J., A. Cornejo, P. Satymurty, C. Nobre, and W. Sea, 1997: Cold surges in tropical and extratropical South America: The strong event in June 1994. *Mon. Wea. Rev.*, **125,** 2759–2786.

Mass, C. F., and N. A. Bond, 1996: Coastally trapped wind reversals along the United States west coast during the warm season. Part II: Synoptic evolution. *Mon. Wea. Rev.*, **124,** 446–478.

Nuss, W. A., and Coauthors, 2000: Coastally trapped wind reversals: Progress toward understanding. *Bull. Amer. Meteor. Soc.*, **81,** 719–743.

Ralph, F. M., L. Armi, J. M. Bane, C. Dorman W. D. Neff, P. J. Neiman, W. Nuss, and P. O. G. Persson, 1998: Observations and analysis of the 10–11 June 1994 coastally trapped disturbance. *Mon. Wea. Rev.*, **126,** 2435–2465.

——, P. J. Neiman, P. G. Persson, J. M. Bane, M. L. Cancillo, J. M. Wilczak, and W. Nuss, 2000: Kelvin waves and internal bores in the marine boundary layer inversion and their relationship to coastally trapped wind reversals. *Mon. Wea. Rev.*, **128,** 283–300.

Reason, C. J. C., and M. R. Jury, 1990: On the generation and prop-

agation of the southern Africa coastal-low. *Quart. J. Roy. Meteor. Soc.*, **116,** 1133–1151.

——, and D. G. Steyn, 1990: Coastally trapped disturbanced in the lower atmosphere: Dynamic commonalities and geographic diversity. *Prog. Phys. Geogr.*, **14,** 178–198.

Rutllant, J., 1981: Subsidencia forzada sobre la ladera andina occidental y su relación con un episodio de contaminación atmosférica en Santiago. *Tralka*, **2,** 57–76.

——, 1983: Coastal lows in central Chile. Preprints, *First Int. Conf. on Southern Hemisphere Meteorology*, Sao Jose dos Campos, Brazil, Amer. Meteor. Soc., 334–346.

——, 1993: Coastal lows and associated southerly winds in north-central Chile. Preprints, *Fourth Int. Conf. on Southern Hemisphere Meteorology*, Hobart, Australia, Amer. Meteor. Soc., 268–269.

——, 1994: On the generation of coastal lows in central Chile. International Centre for Theoretical Physics Internal Rep. IC/94/167, Trieste, Italy, 20 pp.

——, 1997: Day to day wind variability off point Lengua de Vaca (30°15′S, 71°40′W): A simple model. Preprints, *Fifth Int. Conf. on Southern Hemisphere Meteorology*, Pretoria, South Africa, Amer., Meteor., Soc., 120–121.

——, and R. Garreaud, 1995: Meteorological air pollution potential for Santiago, Chile: Towards an objective episode forecasting. *Environ. Monit. Assess.*, **34,** 223–244.

Schemenauer, R. S., H. Fuenzalida, and P. Cereceda, 1988: A neglected water resource: The Camanchaca of South America. *Bull. Amer. Meteor. Soc.*, **69,** 138–147.

Schiffer, R., and W. Rossow, 1985: ISCCP global radiance data set: A new resource for climate research. *Bull. Amer. Meteor. Soc.*, **66,** 1498–1505.

Skamarock, W. C., R. Rotunno, and J. B. Klemp, 1999: Models of coastally trapped disturbances. *J. Atmos. Sci.*, **56,** 3349–3365.

Vera, C. S., and P. K. Vigliarolo, 2000: A diagnostic study of cold-air outbreaks over South America. *Mon. Wea. Rev.*, **128,** 3–24.